Figure S1. The map shows the crater density (for craters larger than 25 km in diameter, N(25), per 10^6 km^2) on Mercury calculated in a moving neighborhood of radius 500 km, updated on the basis of MESSENGER orbital data from [5]. The areas of lowest crater density are smooth plains in the region around the Caloris basin (0° to 60°N, centered on 160°E) and the northern smooth plains (50° to 90°N, centered at 65°E). The areas with highest crater density are north and east of Caloris (NHCT), and at southern high latitudes (SHCT). Both regions are schematically indicated on the map. The map is in an equidistant cylindrical projection centered at 180°E.
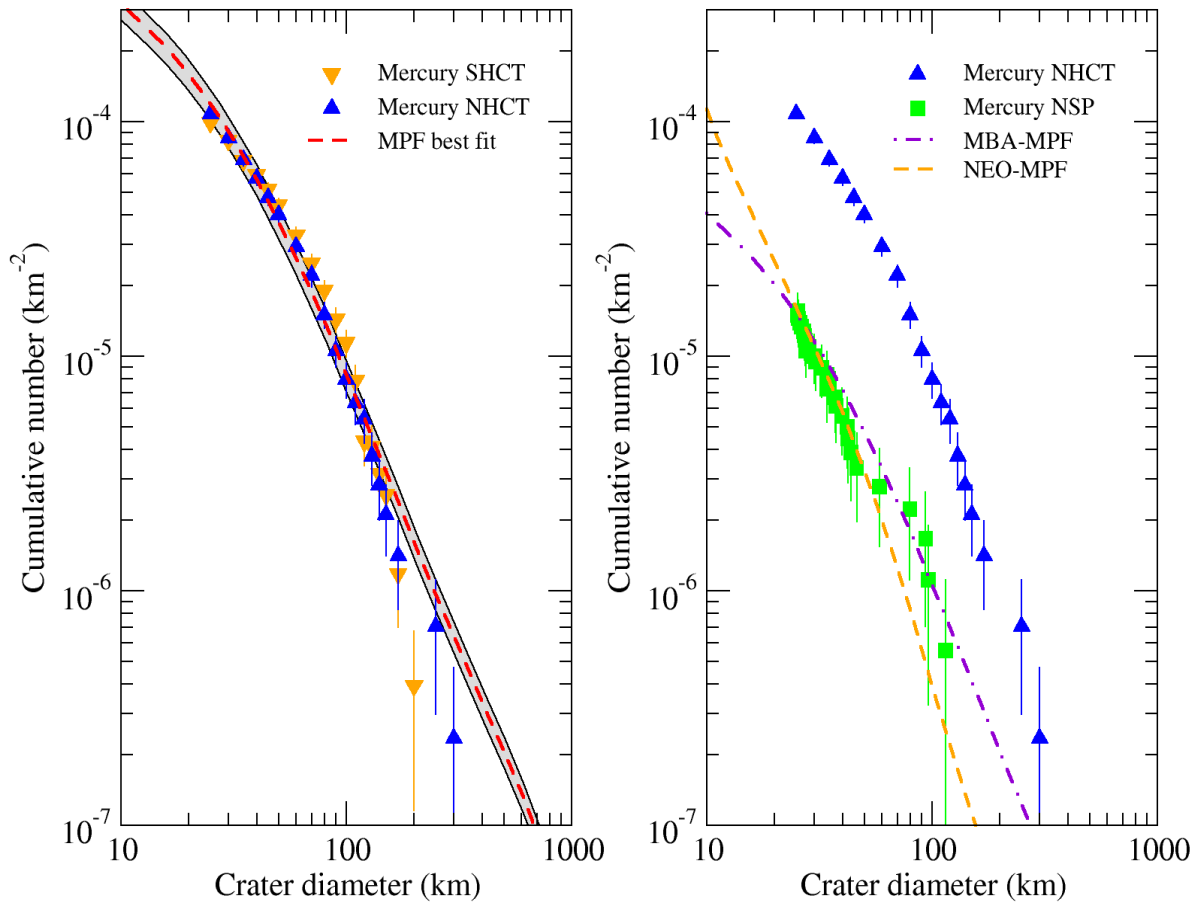
Figure S2. Left panel: Northern and southern heavily cratered terrains (NHCT, SHCT) cumulative size-frequency distributions (SFDs). The two distributions are very similar, and we restrict our analysis to NHCT which seem least affected by the presence of nearby basins. The dashed red curve is the Model Production Function (MPF) best weighted fit to the NHCT [7]. The MPF was obtained using the main belt asteroid SFD and the Pi-group crater scaling law for hard rock [32]. A density of 2.8 g/cm³ and 2.6 g/cm³ has been adopted for both the Mercury upper crust (the same value is used for the Moon) and impactors, respectively [7, 28, 33] (see Fig. S3 for additional details). The gray area shows a region corresponding to 15% variation from the best fit curve; it embraces most of the scatter of the NHCT crater SFD data points. The MPF fits the data well (only the largest size bin is not fitted by the MPF, but this is certainly due to poor statistics), implying that the assumed model can be successfully used to study the early cratering on Mercury. Notably, the current fit is better than the fit to the crater SFD for Mercury's cratered terrains derived from Mariner 10 [1, 3, 33], which on average are more drastically affected by intercrater plains volcanism than our NHCT. **Right panel:** Comparison of NHCT crater SFD to the crater SFD of the northern smooth plains (NSP; data from [16]). The latter shows a steeper slope respect to our main belt asteroid-like MPF (MBA-MPF), revealing a transition to a steeper near-Earth object-like SFD (NEO-MPF), as discussed in previous work [e.g. 19]. The NSP crater SFD may also be affected by episodes of partial erasure given the volcanic nature of these units. For these reasons, the age estimate of NSP is more problematic. In Fig. 3, we show a range of N_{20} values corresponding to the NEO-MPF and MBA-MPF.

On the issue of crater saturation.

An argument that the units presented in Fig. 2 are the production population is that they differ from and have a lower density of craters than saturated terrains. Hartmann [23] observed that the most heavily cratered surfaces on different planetary bodies do not exceed R=0.2-0.3, and that two densely cratered lunar terrains have crater SFDs that plot as a horizontal line in a relative plot having R~0.3, characteristic of what is usually referred to as "empirical saturation". A more recent work [5] confirmed that the most heavily cratered lunar terrains have this shape and R-values of ~0.3, at least for 30<D<100 km, where D is the crater diameter. These crater densities are significantly higher than the crater SFD for the lunar pre-Nectarian terrains in Fig. 2. For this reason, unless saturated surfaces can exist with significantly lower densities and a different size-frequency distribution, the pre-Nectarian crater SFD (and therefore NHCT) is not likely to be saturated for 20<D<100 km. Indeed, one readily observes that craters on the NHCT are not closely packed but separated by intercrater plains.

On the other hand, if the production SFD is dominated by large craters, heavily cratered terrains can be in a quasi-steady-state of saturation exhibiting a crater SFD that resembles the production function and falls below R=0.3 at smaller diameters [20, 34, 35]; however, we do not see much evidence for erasure of smaller craters by larger ones in the NHCT. Yet another possibility is that the formation of intercrater plains, which are visible even in the NHCT, has been responsible for part of the downturn in density for smaller craters. Such modification is, however, unlikely to have significantly altered the NHCT crater SFD given that it provides a good fit to the Model Production Function (see Figs. S2, S4 for additional information).

Rescaling the lunar impactor flux to Mercury.

To compare the impact flux striking the Moon with that of Mercury (Fig. S3), we examined the dynamics of small bodies in the present-day inner solar system using the results of [24, 25]. We assumed that the vulcanoid population, the hypothesized small body population that predominantly hits Mercury [e.g. 36], was not a factor in our calculations. We also assumed that the impactors striking Mercury and the Moon mainly came from the main belt region, as suggested by recent models for the Late Heavy Bombardment (LHB) [25]. This implies that the same source population is making visible craters and basins on Mercury and the Moon, although the relative contributions differ according to the orbital distributions of the impactors. Here we adopt the approach described in [7, 37] for computing a scaling factor to compare crater densities on Mercury with that of the Moon. We use numerically generated populations of Moon- and Mercury-crossing asteroids to compute the intrinsic collision probabilities between these bodies and the Moon to Mercury ratio [7, 37]. We also used a main belt like size-frequency distribution (see Fig. S2) that was rescaled to the current number of near-Earth objects at 1 km. The resulting cumulative number of impacts by asteroids ≥1 km are $1.27 \ 10^{-15}$ $yr^{-1}km^{-2}$ and $7.37 \ 10^{-16}$ $yr^{-1}km^{-2}$, respectively, for Mercury and the Moon. This implies that the impact flux ratio for Mercury vs. the Moon (per km^2) is 1.72. This ratio is very similar to the one obtained using the debiased near-Earth object population by [24] and also to a value found using an independent computation by [18]. Finally, we use crater scaling relationships to account for higher impact velocities at Mercury vs. the Moon, which average 42 km/s and 19 km/s, respectively [7]. Fig. S3 reports the MPF for two different crater scaling laws (SL1 [30]; SL2 [38]).
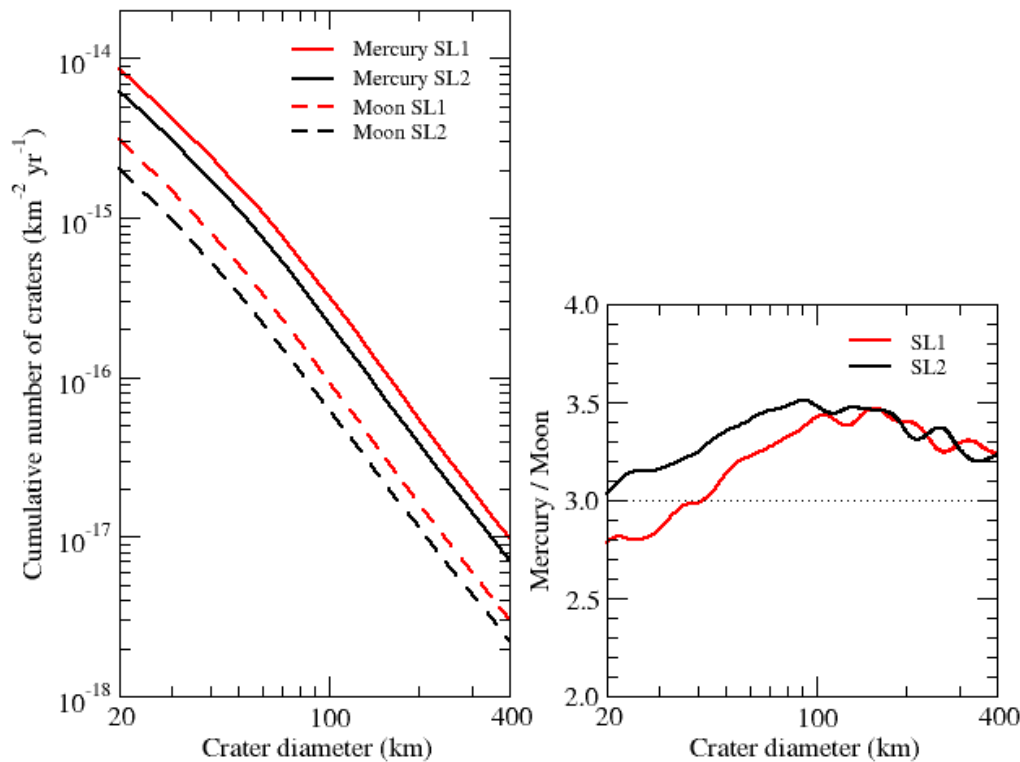
Figure S3. Left panel: Model Production Functions (MPF) for the Moon and Mercury. These plots were derived by accounting for the differences between Mercury and the Moon concerning impact velocities, gravitational focusing, and crater scaling laws. **Right panel:** The ratio of the Mercury and lunar model production functions. On average, ~3-3.5 times as many craters in the size range relevant for this work (20-300 km) should form on Mercury as on the Moon. We adopt the factor of 3 in this work.

On the age assessment of Mercurian terrains.

It is interesting to compare our rescaling factor with those estimated by others. A recent work [18] estimates a rescaling factor of about 3.4 (averaged over the size range 20-300 km, which is relevant for our purposes; see their Fig. 3); this would produce a slightly younger age (of the order of 50 Myr) for the Mercury NHCT. This result is within the error bars of our own estimate.

An earlier work [4] estimated that the scaling factor to be ~1.1 (at D=1 km, since their chronology is based on the cumulative number of craters at 1 km), so the age of terrains on Mercury would be significantly older than computed here. There are, however, two major problems with this estimate.

The first one is that their scaling was based on a catalog of near-Earth objects (NEOs) (from Lowell Observatory in 2000) that underestimated the number of objects on Mercury-crossing orbits. For example, their Fig. 8 (left-hand panel) shows that 25-70 NEOs are on Mercury-crossing orbits, while about 500 are on Earth/Moon-crossing orbits. The debiased numbers of absolute magnitude H<18 objects estimated from [24] are 221 and 694, respectively. So the ratio of Mercury-crossers to Moon crossers is <0.14 (=70/500) for [4], while the current debiased ratio is ~0.31 (=221/694). This leads to a value that is about 2.3 times larger than what was estimated by [4].

The second problem is that [4] computed a significantly lower average impact velocity for projectiles with Mercury (32.2 km/s, see their Fig. 9) than found by more modern estimates, which give ~42 km/s [7, 18, 37]. By coupling this information with the crater scaling law (crater size scales as $v^{0.44}$, where v is the impact velocity), one can compute that the vertical shift of the crater production function is about 1.3 (assuming a -2 power-law cumulative slope). Both factors play a role in computing the ratio of the crater density at a given crater size. The total corrected scaling factor would, therefore, be 1.1x2.3x1.3~3.3, in agreement with our estimate and that of [18].

In the light of these results, the fact that previously published age estimates for the oldest terrains on Mercury based on Mariner 10 data [3,4] concluded that those terrains were ~4 Gyr old is likely due to a coincidental compensation of the several factors involved in those estimates. Moreover, those early chronologies assumed an exponential smooth decay of the impactor flux, resulting in an artificial "compression" of ages around ~4 Gyr ago because the crater density on a given terrain cannot indefinitely increase [6].
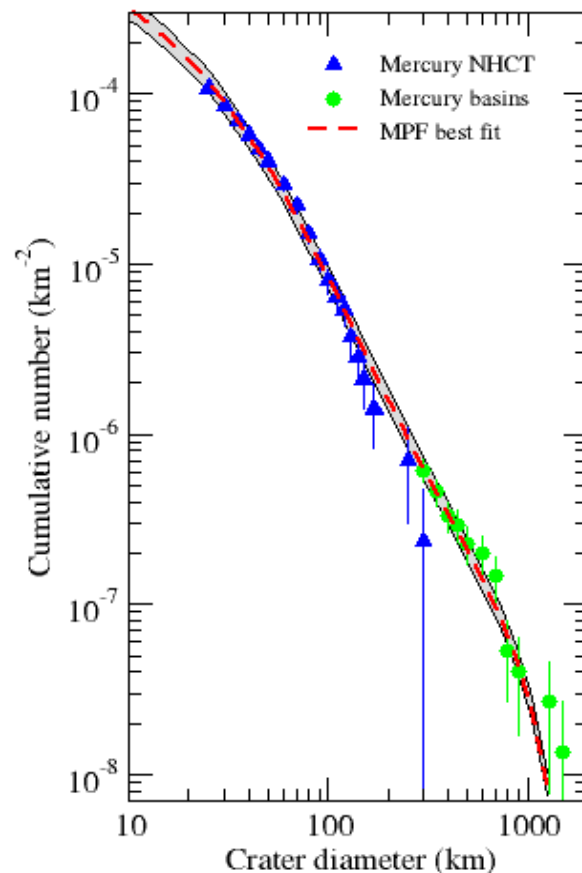

Figure S4. Comparison between NHCT crater SFD and large basins SFD (derived from the list of certain and probable basins given in [8]). The MPF from Fig. S2 is also plotted, showing an overall remarkably good fit from ~25 km to ~1000 km crater diameter. This is strong indication that a main belt-like impactor SFD produced the oldest visible craters and basins. Also, the fit shows that the age of the entire surface is about the age computed for NHCT, namely 4.0-4.1 Gyr ago. Moreover, since the spatial density of large basins is arguably below empirical saturation, R<0.15 [8], the fact that their SFD lines up with the NHCT crater SFD is an additional indication that the NHCT is not saturated.

Crater (km)	Cumulative (km^{-2})	Error (km^{-2})
25	1.08E-04	5.04E-06
30	8.51E-05	4.47E-06
35	6.87E-05	4.01E-06
40	5.72E-05	3.66E-06
45	4.74E-05	3.33E-06
50	4.01E-05	3.07E-06
60	2.93E-05	2.62E-06
70	2.20E-05	2.27E-06
80	1.50E-05	1.88E-06
90	1.06E-05	1.57E-06
100	7.97E-06	1.37E-06
110	6.33E-06	1.22E-06
120	5.39E-06	1.12E-06
130	3.75E-06	9.38E-07
140	2.81E-06	8.13E-07
150	2.11E-06	7.04E-07
170	1.41E-06	5.75E-07
250	7.04E-07	4.06E-07
300	2.35E-07	2.35E-07

Table S1. Diameter, cumulative numbers and error bars for the NHCT crater SFD. The counted area is 4.26 10^6 km^2.

References

[32] Melosh H. J. Impact cratering: A geologic Process. Oxford Monographs on Geology and Geophysics, no. 11, Clarendon Press, Oxford, (1989).

[33] Massironi, M., Cremonese, G., Marchi, S., et al. Mercury's geochronology revised by applying the Model Production Function to Mariner 10 data: Geological implications. GRL 36, 21204 (2009).

[34] Chapman, C.R., McKinnon,W.B. Cratering of planetary satellites. Satellites (A87-23307 09-91). Tucson, AZ, University of Arizona Press, 1986, p. 492-580. NASA-supported research (1986).

[35] Richardson, J.E. Cratering saturation and equilibrium: A new model looks at an old problem. Icarus 204, 697-715 (2009).

[36] Steffl, A.J. et al. A search for Vulcanoids with the STEREO Heliospheric Imager. Icarus 223, Issue 1, 48-56 (2013).

[37] Marchi, S., Morbidelli, A., & Cremonese, G. Flux of meteoroid impacts on Mercury. A&A, 431, 1123-1127 (2005).

[38] Holsapple, K.A., and Housen, K.R. A crater and its ejecta: an interpretation of deep impact. Icarus 187, 345-356 (2007).